# Modification of dispersion, localization, and attenuation of thin metal stripe symmetric surface plasmon-polariton modes by thin dielectric layers

Ronen Adato[a] and Junpeng Guo[b]
*Department of Electrical and Computer Engineering, University of Alabama in Huntsville, Huntsville, Alabama 35899, USA*

(Received 2 October 2008; accepted 12 December 2008; published online 5 February 2009)

We systematically investigated the properties of the fundamental symmetric surface plasmon-polariton mode supported by a finite width gold microstripe with thin dielectric layers placed above and below it. This paper describes the dispersive behavior of the fundamental symmetric mode and the dependence of its attenuation and confinement on the thin dielectric layers' thickness and refractive index. When the dielectric layers have a refractive index less than that of the cladding, the dispersion curve shifts toward the cladding light line and the mode attenuation is reduced with the tradeoff of reduced confinement. For dielectric layers with an index of refraction higher than that of the cladding, the dispersion curve shifts away from the cladding light line and the mode confinement is enhanced at the cost of increased attenuation. When designed properly, the higher refractive index dielectric layers in combination with the low index cladding can achieve tight mode confinement which cannot be obtained by using either a high or low index homogeneous dielectric cladding. The dependence of the mode's properties on the thickness and width of the metal stripe and dielectric layers is also investigated. © *2009 American Institute of Physics*.
[DOI: 10.1063/1.3073991]

## I. INTRODUCTION

Surface plasmon polaritons (SPPs) are electromagnetic waves coupled to the coherent oscillations of a metal's free electron density and propagate along the metal-dielectric interface. These bound surface waves provide an alternative mechanism with which to localize and guide optical frequency electromagnetic radiation different from the total internal reflection mechanism that optical fibers and traditional dielectric waveguides rely on. The single interface between a semi-infinite metal and a semi-infinite dielectric medium supports one bound SPP mode which has a very large propagation attenuation in visible and infrared frequencies.[1] Thin metal films typically support two bound SPP modes, one of which has relatively low propagation attenuation and is thus called the "long range surface plasmon-polariton mode."[2–6] Finite width metal stripe surface plasmon-polariton waveguides, which provide two dimensional mode confinement, are of greater practical interest. Two dimensional structures support a number of bound modes depending on the metal stripe width, thickness, material properties, and the wavelength.[7–12] The fundamental even field symmetric[13] mode ($ss_b{}^0$ in the notation of Refs. 7 and 8 and hereafter) supported by metal stripes embedded in a homogeneous dielectric medium has been of interest regarding the design of SPP based photonic components. Two important characteristics are its relatively long propagation ranges (in comparison with those of other SPP waveguide geometries) and that the spatial distributions of its dominant fields resemble a Gaussian profile, therefore allowing efficient end-fire coupling to and from optical fibers.[4,14,15] Key plasmonic optical components such as couplers,[16,17] *y*-junctions,[15,17] Bragg gratings,[18,19] modulators, and switches[20,21] have been demonstrated.

The dielectric media in the one dimensional single interface and thin film SPP guide geometries are homogeneous and occupy the semi-infinite upper and lower spaces. Finite width metal stripe guide SPP geometries are typically embedded in homogeneous dielectric backgrounds or supported by a high index substrate while a lower index dielectric occupies the upper half space. Recent work has shown, however, that placing thin additional dielectric layers at the surfaces of the metal offers a means with which to modify the dispersion, confinement, and attenuation of the plasmon modes. Through changes in the refractive index and thickness of the dielectric layers these characteristics can be varied. Slow and negative group velocities have been predicted for thin high index (with respect to the semi-infinite homogeneous cladding) layers placed at the surface of a semi-infinite metal slab described by a lossless Drude-free electron model (neglecting the damping term),[22] although these modes were shown to suffer from severe attenuation.[23] Finite difference time domain (FDTD) calculations describing a means of exciting the mode have also been reported.[24] The possibility of using the thin dielectric layers to tailor the mode confinement and propagation range of the SPP modes supported by a thin gold film was first investigated in Ref. 25. Depending on whether the refractive index of the dielectric layers was higher or lower than that of the cladding, increasing the thickness of the dielectric layers was shown to result in two different types of behavior. For high index of refraction dielectric layers, the real part of the mode index

[a]Present address: Department of Electrical and Computer Engineering, Boston University, Boston, MA 02215.
[b]Author to whom correspondence should be addressed. Electronic mail: jguo@ece.uah.edu.

 

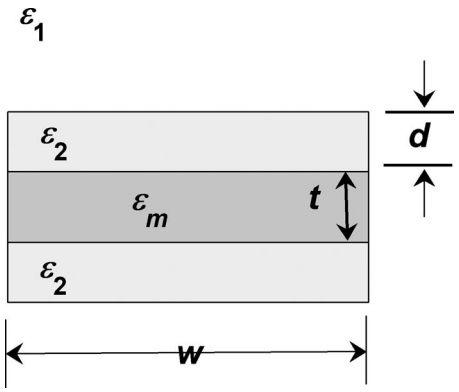


FIG. 1. The two dimensional cross section of the layered metal-dielectric SPP waveguide.

was seen to increase with the thickness of the dielectric layers while the propagation range exhibited a small local minimum. Additional modes were also seen to appear with increases in the thickness of the dielectric layers. In contrast, dielectric layers with smaller index of refraction than that of the cladding, can significantly extend the propagation range of the symmetric mode up to the cutoff as the dielectric layer thickness is increased. Confinement, however, is reduced as the mode index is made to approach the refractive index of the cladding dielectric. The behavior of these ultralong range modes was examined in greater detail for different thicknesses of the metal film, dielectric layer refractive indices, and wavelengths.[26] Increases in the mode's spatial extent were also noted[27] and similar effects were also shown to be present for the fundamental symmetric mode supported by a finite width metal stripe.[28] Although the mode delocalization in this case is in general undesirable—the adverse effects of air gaps[29,30] are essentially extreme examples of this geometry—under certain circumstances should an application or component design require a stripe or film that is thicker than propagation range constraints allow, for instance, the ability to slightly relax such constraints would prove useful. Recently, it has been pointed out that when placed at the top and bottom surfaces of thin metal films and about a finite width metal stripe,[31] the high index dielectric layers allow for the excitation of modes with characteristics that are desirable for application to optical circuit design. The redistribution of the mode's fields inside the high index layers allows for the possibility of improved energy localization, which have been shown to reduce the 90° bend loss in numerical simulations[31,32] and later realized experimentally.[33]

In this paper, we systematically investigate the general behavior of the fundamental symmetric bound mode supported by the structure whose two dimensional cross section is shown in Fig. 1. The frequency dependence of the mode's propagation constant is examined in detail for waveguides with both the high and low index dielectric layers in Sec. III. It is shown that high index dielectric layers shift the SPP dispersion curves away from the cladding light line and as a result mode confinement is improved at the cost of increased attenuation. Low index dielectric layers shift the dispersion curves in the opposite direction toward the cladding light line. The result is that attenuation is reduced along with mode confinement and for certain combinations of wavelength, material properties, and guide geometry the mode is cut off. The mode confinement and attenuation characteristics are examined as a result of variations in the dielectric layer refractive index in Sec. IV and then as functions of their thickness in Sec. V for both high and low refractive index dielectric layers. A significant result discussed in Sec. V is that, beyond the improved confinement implied by the dispersion curve shifts seen for the high index layers in Sec. III, exists an optimal thickness of the high index dielectric layers that allows for the mode's fields to be localized to an area smaller than is achievable with either the high or low index homogeneous cladding. The effect is also considered for different metal stripe thicknesses since the properties of the $ss_b^0$ mode are known to vary considerably with the metal stripe thickness for relatively thin metal stripes (i.e., the top and bottom metal-dielectric interfaces are still coupled). Finally, the effects of changes in the metal stripe and dielectric layers' width are considered in Sec. VI for both high and low index dielectric layer waveguides. The high index layer configuration is characterized by strong confinement here as well, allowing for relatively narrow stripes to guide tightly bound modes, while for the low index case strong deviations in the mode properties are found even for wide stripes as a result of the reduced confinement. In this manner, we aim to provide a quantitative description of the range of effects achievable with the additional dielectric layers, which offer clear advantages over finite width metal stripe guides embedded in purely homogeneous claddings.

## II. WAVEGUIDE GEOMETRY, MATERIAL MODEL, AND NUMERICAL METHOD

In order to examine the behavior of the fundamental field symmetric mode supported by the structure shown in Fig. 1, the propagation constants were calculated at different wavelengths, dielectric layer refractive indices and thicknesses, and thicknesses and widths of the metal stripe. The mode described reduces to the $ss_b^0$ described in Refs. 7 and 8 if the dielectric layer thickness $d$ is reduced to zero and maintains the same field symmetry; therefore no distinction will be made in the notation of this paper. Throughout the calculations and the discussion to follow, the coordinate axes are such that the $x$-axis is coincident with the horizontal axis of symmetry and the $y$-axis is taken to lie along the vertical axis of symmetry of the metal stripe. Propagation is in the $z$-direction with the dependence on $z$ as $\exp(-j\gamma z)$, where $\gamma=\beta-j\alpha$. The free space wave number is $k_0=2\pi/\lambda$. Several metrics are used in examining the behavior of the mode, including propagation range $[1/(2\alpha)]$, confinement in terms of distance from the cladding light line $(\beta/k_0-n_1)$,[34] and the spatial extent[35,36] of the mode fields. The spatial extent in the two dimensional case here is defined in analogy with the one dimensional measure in Ref. 34 as the total distance in between the two $1/e$ decay points of the mode's dominant transverse magnetic field component $(H_x)$ taken along a cross sectional cut passing through the point of maximum field amplitude. Cuts are therefore taken along the $y$-axis to mea-

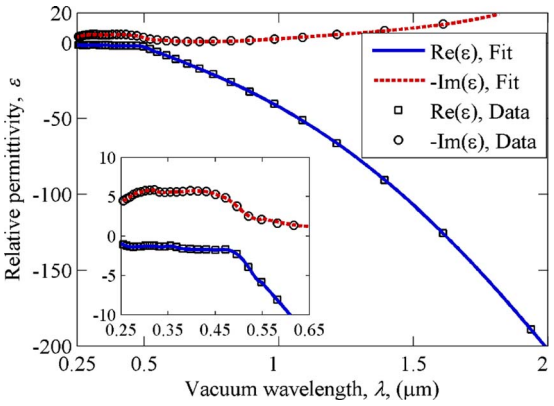


FIG. 2. (Color online) The real and imaginary parts of the relative permittivity of gold are plotted as the function of the wavelength from 250 nm to 2 $\mu$m. The inset shows in greater detail the material dispersion in the visible and UV ranges.

sure vertical spatial extent and along the top (or equivalently bottom, given the symmetry of the structure) long edge of the metal stripe to measure lateral spatial extent. In all cases examined here, the metal is gold. Its permittivity is taken as a complex number $\varepsilon_m = \varepsilon_m' - j\varepsilon_m''$, while all the dielectrics are taken to be lossless, hence their permittivities are purely real. In order to account for the frequency dependence of the dielectric response of gold, its relative permittivity at a given wavelength was taken from Johnson and Christy's data,[37] as shown in Fig. 2. Following Ref. 38, a fourth order polynomial fit to the data between the ranges of 0.55 and 2 $\mu$m was used for the interpolation of values in that range and a cubic spline used for wavelengths occurring between 250 and 550 nm. The functions are appropriate strictly for interpolation purposes and no points outside the range of the actual data were used.

The calculation of the mode propagation constants was accomplished using a commercial implementation[39] of the film mode matching method.[40,41] The method is fully vectorial and well suited to yield accurate results to problems where the waveguide cross sectional geometry can be decomposed into a finite number of rectangles, as is the case here, with considerably less computational effort than finite element or finite difference methods. The basis of the method is to decompose the two dimensional cross section into a number of slices, which have refractive index profiles that are invariant along the horizontal and therefore represent one dimensional film guides. The general field in each slice is then represented by a mode expansion. The continuous spectrum of unbound modes is discretized through the introduction of artificial perfect electric ($E_{\text{tangential}}=0$) or magnetic ($H_{\text{tangential}}=0$) conductor walls at the top and bottom boundaries. Transparent boundary conditions (which effectively set the boundary wall at infinity) were used as the left and right boundary conditions. The matching of the fields along a vertical cut where the mode's fields are estimated to be appreciable (the center of the guide for the $ss_b^0$ mode) yields the nonlinear eigenvalue problem to be solved for the mode propagation constant. Key sources of numerical error requiring convergence analysis are the proximity of the artificial top and bottom boundary walls to regions where the mode's fields are not negligible in amplitude and also the number of one dimensional film modes included in the mode expansion in each slice. The two considerations are interrelated in that increasing the distance of the walls from the guiding structure reduces their effect on the solution but increases the size of the computation domain and therefore the number of terms in the mode expansion necessary for accurate results. That the domain was kept as small as possible while keeping the walls acceptably far from the guide core was verified by comparing solutions found for electric and magnetic walls and iteratively expanding the computation domain until the two are equal within a set precision, as suggested in Ref. 40. Straightforward convergence analysis is also possible although increasingly large oscillations in the solution occur if the number of one dimensional modes is kept constant as the wall distance is expanded.[42] Solutions were examined as the number of included film modes was increased to verify convergence. A final boundary condition check was performed following verification of convergence in the number of terms in the mode expansion. In general, convergence in the number of film modes tends to improve convergence in the boundary wall distance as the oscillatory behavior with increasing computational domain size is reduced since the inclusion of a greater number of film modes improves accuracy.[39–42]

## III. DISPERSION EFFECTS

Since the fields and energy density of bound SPPs are localized at the surface of the metal, their wave vectors are very sensitive to refractive index variations occurring there at the point where their field amplitudes are at the maximum. This forms the basis for the placement of the dielectric layers at the surface of the metal to cause variations in the properties of the $ss_b^0$ mode. Of importance to the dispersion of the mode is the fact that the degree to which the fields of SPP modes are concentrated within several nanometers of the surface of the metal is strongly dependent on frequency. For the layered structure discussed here, at low frequencies, much of the mode's fields propagate within the cladding, and the dispersion curve can be expected to lie close to that of the $ss_b^0$ mode of a stripe guide embedded in a purely homogeneous background of the same material as the cladding. As the resonant frequency is approached, increases in the confinement of the mode's fields at the metal's surface increase the proportion of energy propagating within the metal layer. The mode's wave vectors can then be viewed as approaching the values they would take on were the dielectric layers made infinitely thick.

### A. High index dielectric layers

Dispersion curves calculated for the $ss_b^0$ mode supported by the guide with high index dielectric layers are shown in Fig. 3. The gold stripe is 1 $\mu$m wide by 20 nm thick, and the thickness of the dielectric layers is held constant at 50 nm throughout. The cladding refractive index is 1.50 and curves are shown for $n_2=1.50$, 2.00, 2.50, and 3.00, the first of these (black diamonds in the figure) representing the case without the dielectric layers. In all cases, dispersion curves are

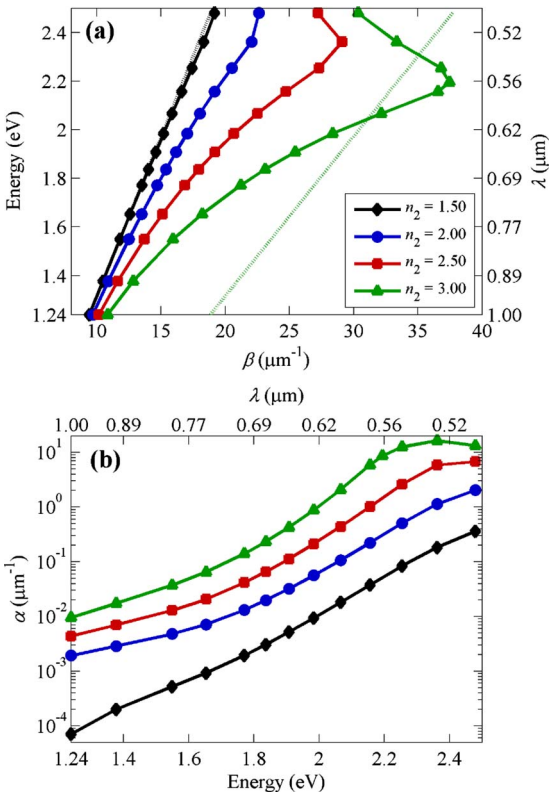


FIG. 3. (Color online) Dispersion curves for high index dielectric layers. The index of refraction is varied as shown in the legend of (a), which also applies to (b), while all other parameters are held constant. The dotted black line is the cladding light line.

shifted away from the cladding light line, and the high index dielectric layer leads to a reduction in the resonant frequency and both the group and phase velocity of the mode. At low frequencies, the modes' wave vectors lie close together along the cladding light line as their fields are predominantly concentrated in the cladding material. With increasing frequency, the transition to the $d=\infty$ case is evident in the reduction in the resonant frequency for the higher refractive index dielectric layers. In addition, the wave vector on resonance is enhanced for higher dielectric layer refractive indices. In general, SPPs propagating along metal surfaces exhibit enhanced resonances for higher index of refraction embedding media. Additionally, as can be seen in the inset of Fig. 2, a shift in the resonant frequency to longer wavelengths reduces the imaginary component of the relative permittivity of gold responsible for the damping of the resonance, despite the fact that a Drude model, even if it includes loss, predicts it to be a strictly decreasing function of frequency.

As increasing the index of refraction of the high index dielectric layers, an increase in attenuation ($\alpha$) is observed in Fig. 3(b) as a result of the increase of the real part of the propagation constant ($\beta$) as shown in Fig. 3(a) and the implied higher concentration of the mode's fields within the dissipative metal. We note, however, that although the increased distance from the cladding light line implies a tighter mode confinement as a result of an increased rate of exponential decay of its fields in the cladding, additional effects result from the different forms of the fields inside the dielectric layers. These effects are investigated in Sec. V. The position of the dispersion curve with respect to the light line of the high index dielectric layers is of interest in this regard as it determines the functional form of the dependence of the mode's field distribution on the $y$ coordinate. The light line for $n_2=3.00$ is shown as the green dotted line in Fig. 3(a). At lower frequencies the corresponding dispersion curve lies to the lower momentum side of the dielectric layer light line. The field dependence with distance from the metal surface inside the dielectric layers is therefore approximately a linear combination of cosine and sine functions. Although these modes, to a certain extent, can be thought of as hybrid SPP/dielectric waveguide modes, the dispersion curve behavior with increasing frequency can be seen to much more closely resemble that of a pure SPP. Eventually, the dispersion curves do cross over the dielectric layers' light line and the functional form of the field distribution is approximately a linear combination of decaying and growing exponentials. The simulation results shown correspond to a thin 20 nm thick metal stripe. Since increasing the thickness of the metal stripe increases the $ss_b^0$ mode wave vector, the dispersion curves and fields of mode for thicker metal stripes will be much more closely related to those of a pure SPP over a wider range of frequencies. Finally, although the region of anomalous dispersion is made larger and reduced in frequency, modes here are highly damped, as is seen in Fig. 3(b), making their practical investigation difficult.

The dispersive behavior of the $ss_b^0$ mode shown in Fig. 3(a) is similar to that of a semi-infinite metal slab (one dimensional) at whose surface thin dielectric layers were placed.[22] The differences here are, first, realistic material permittivity model is used for the metal (as opposed to a Drude model without damping), which results in finite wave vectors on resonance, rather than the approach to infinity when damping is neglected. Second, the fields of the $ss_b^0$ mode supported by thin metal stripes are less tightly confined to the metal's surface than those of the single interface of a semi-infinite metal slab. The result is that the dielectric layers used here can be relatively thick and the transition in the dispersion curves to the $d=\infty$ case is not usually as complete in comparison with the calculations in Ref. 22.

### B. Low index dielectric layers

In contrast to high index dielectric layers, ones that are less optically dense than the cladding will shift the dispersion curve toward the cladding light line. The effect is shown in Fig. 4 where the guide without the dielectric layers is compared to one with 50 nm thick $n_2=1.45$ layers. All other material and geometry parameters are the same as in the previous section. The inset shows the behavior about the SPP resonance in greater detail. The increase in wave vector on resonance is small for both curves as a result of the high absorption of gold. Additionally, the lower index dielectric layers shift the resonance to slightly higher frequencies, where absorption is greater, damping it further. The incremental movement of the dispersion curve toward the cladding light line results in greatly reduced mode confinement and therefore much lower propagation losses. The effect is

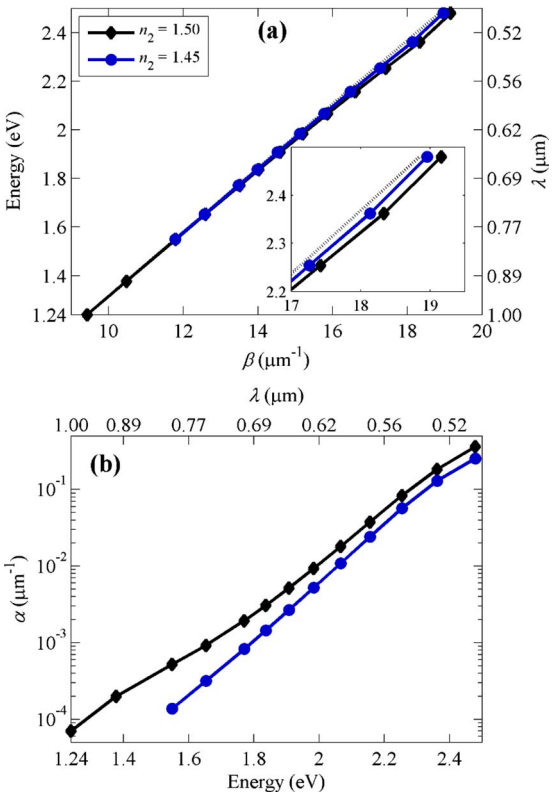


FIG. 4. (Color online) (a) Dispersion and (b) attenuation curves for the low index dielectric layer case. The legend shows the dielectric layer refractive index and all other parameters are the same as in Fig. 3. The inset clarifies the behavior near the resonance. The cladding light line is shown as the black dotted line in (a).

made larger at longer wavelengths, where the wave vectors of the mode without the inner layer are already very close to the cladding light line. As a result, as wavelength is increased, a point where the shift drives the mode index over the light line and the mode becomes unbound and cutoff is reached. The approach to cutoff is visible in Fig. 4(b) as attenuation can be seen to be reduced drastically at the lower energies. At wavelengths around 900 nm (not shown) the mode becomes highly delocalized. Further into the near IR, the mode is cut off.

As a final matter, we mention here that increasing the contrast between the cladding and the dielectric layers increases the shift in mode wave vector toward the cladding light line. Cutoff and the associated reductions in attenuation thus occur at shorter wavelengths. Such behavior is similar to the case of one dimensional guide in Refs. 25 and 26. Section IV illustrates the extension to the two dimensional case. The low index dielectric layers thus offer a relatively robust means to extend the propagation range of the $ss_b^0$ mode in applications where confinement is not critical. Other methods of improving propagation range include embedding the metal in an asymmetric dielectric environment, usually with a high index dielectric substrate, and a low index superstrate.[43,44] A method has also been described, for a one dimensional geometry, whereby an additional set of dielectric layers is placed above the metal film, such that a portion of the SPP mode's fields propagate in an adjacent dielectric waveguide, can also achieve increased propagation ranges.[45]

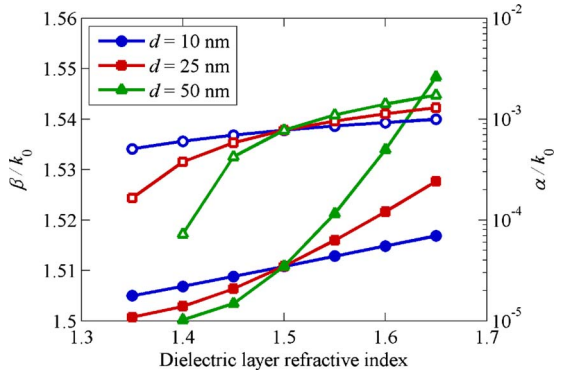


FIG. 5. (Color online) Real ($\beta/k_0$, filled markers) and imaginary ($\alpha/k_0$, open markers) parts of the mode index are plotted on the left (linear scale) and right (logarithmic scale) hand axes, respectively. The curves correspond to dielectric layer thicknesses of 10, 25, and 50 nm as indicated.

Such methods do not, however, maintain the symmetry of the mode desirable for fiber coupling as mentioned and confinement is sacrificed similarly.

## IV. DEPENDENCE OF MODE PROPERTIES ON THE REFRACTIVE INDEX OF THE DIELECTRIC LAYERS

The effects of variations in the refractive index as well as the thickness of the dielectric layers on the mode index ($\gamma/k_0$) are illustrated in Fig. 5 for a set wavelength. Mode indices were calculated at $\lambda$=633 nm ($\varepsilon_m$=−11.65−$j$1.33) for dielectric layer thicknesses of 10, 25, and 50 nm as their refractive index was stepped through values between 1.35 and 1.65. The cladding refractive index was held fixed at 1.50 and the gold stripe thickness and width were set at 20 nm and 1 $\mu$m, respectively. In general, shifts in the refractive index of the dielectric layers to values larger than $n_1$ (high index dielectric layers case) result in increases in the real part of the mode index and, as will be seen, mode confinement, while propagation range is slightly reduced, as indicated by the increase in the imaginary part of the mode index. As was seen in the discussion of dispersion for the high index dielectric layer case, increasing the refractive index of the dielectric layers shifts the mode's propagation constant progressively further from the cladding light line. As the refractive index of the dielectric layers is reduced below that of the cladding (low index dielectric layers case), effects indicative of the dispersion curve shift toward the cladding light line are observed in the reductions in both the real and imaginary parts of the mode index. As with the high index dielectric layers, increasing the contrast between the dielectric layers and the cladding results in large shifts in the mode's propagation constant, this time toward the cladding light line. Although only the dispersion curve for $n_2$=1.45 was plotted in Sec. III, the behavior (overall shift in the dispersion curve toward the cladding light line and cutoff occurring at increasingly shorter wavelengths) for lower refractive index dielectric layers can be inferred when taken in conjunction with the results in Fig. 5 for a single wavelength. With reduced dielectric layer refractive indices, the real part of the mode index approaches the refractive index of the cladding (until cutoff is reached) while at the same time large

reductions in the imaginary part of the mode index occur, which imply greatly reduced propagation losses.

For both cases, high and low index dielectric layers, the curves for the different dielectric layer thicknesses imply a general increase in the size of the effects discussed in the preceding paragraph with increasing dielectric layer thickness. For a given shift in the refractive index of the dielectric layers to the high index side of $n_1$, the resulting increase in the real part of the mode index is larger for thicker dielectric layers. Although for all the curves shown in Fig. 5 the imaginary part of the mode index increases with the thickness of the dielectric layers as well, Sec. V will show that this is not always the case. The heterogeneous refractive index profile in the $y$-direction results in different decay rates and forms of the mode's field distributions inside the dielectric layers and the cladding. In general it will be shown that the concentration of the mode's fields in and about the metal stripe, as a function of the dielectric layers' thickness, does not vary in the same way as the mode's propagation constant's distance from the cladding light line. Neither then does the imaginary part of the mode index, which is a function of the concentration of the mode's fields inside the lossy metal. As the index of refraction of the dielectric layers is reduced to values below that of the cladding, for thicker dielectric layers the effect is again greater with the cutoff and the large decreases in the imaginary part of the mode index associated with the approach to it occurring for smaller reductions in the dielectric layer refractive index. For both 10 and 25 nm thick dielectric layers the mode is bound at $n_2=1.35$. For the 50 nm thick layer, however, the mode is already very loosely bound at $n_2=1.40$ and is cut off roughly in the vicinity of $n_2=1.35$.

It has been mentioned that the tradeoff made in the high index dielectric layer case is the reduction in propagation range in exchange for improvements in mode confinement. For low index dielectric layers, the converse is true with gains in propagation range at the expense of mode localization being possible. The calculations of the mode index in Fig. 5 describe the effects in terms of the propagation range and distance from the cladding light line. Where the dielectric layers are not present, the $ss_b^0$ mode is characterized by a propagation range of 65 $\mu$m and distance from the light line of $1.1\times10^{-2}$. With 50 nm thick dielectric layers, increasing the refractive index to 1.60 reduces the propagation range to 36 $\mu$m but also results in a greater than threefold improvement in the light line distance, raising it to $3.4\times10^{-2}$. By reducing the dielectric layer thickness, the propagation range is increased to 120 $\mu$m at the cost of reducing the light line distance metric to $3.4\times10^{-3}$, an order of magnitude smaller than for the 1.60 refractive index inner layer. It is interesting to note that the relevant figure of merit discussed in Ref. 34 $[(\beta/k_0-n_1)/(2\alpha)]$ considers the $n_2=1.60$ guide to be the most favorable of the three.

The actual spatial extent of the mode's field distribution should also be considered as it determines the pitch between adjacent waveguides, an important characteristic for the design of optical interconnects for example. We have noted that although both distance from the cladding light line and mode spatial extent often vary together, this is not always the case here as a result of the heterogeneous refractive index profile. The effects of variations in the dielectric layer refractive index on the distribution of the mode's fields are considered directly in Fig. 6. The profiles of the dominant transverse magnetic field for the three cases discussed, $n_2=1.50$, 1.60, and 1.45, are shown in Figs. 6(a)–6(c), respectively. The increase in mode confinement for the high index dielectric layers in Fig. 6(b) is especially striking, a feature which will be a key point in Sec. V and will be discussed in detail. The $1/e$ contours of the $H_x$ field are compared directly in Fig. 6(d) and the corresponding values of the spatial extent in the $y$ direction are 0.84, 0.56, and 1.2 $\mu$m for $n_2=1.50$, 1.60, and 1.45, respectively. Confinement in the $x$ direction follows the same trend with values of 1.2, 1.1, and 1.5 $\mu$m for $n_2=1.50$, 1.60, and 1.45, respectively.

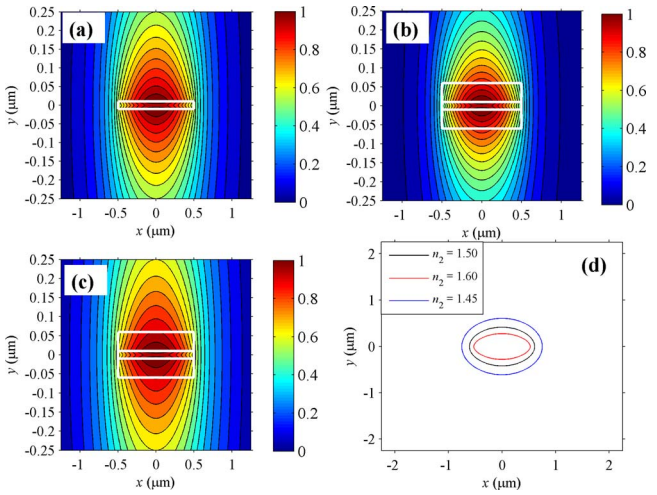


FIG. 6. (Color online) Mode profiles of the $H_x$ field for 50 nm thick dielectric layers. In (a), the refractive index of the dielectric layers is 1.50, the same as that of the cladding, equivalent to there being only a purely homogeneous background. In (b) $n_2=1.60$, and in (c) $n_2=1.45$. The outlines of the metal stripe and the dielectric layers are shown in white. The $1/e$ contours of $H_x$ are compared in (d).

## V. DEPENDENCE OF MODE PROPERTIES ON THE THICKNESS OF THE DIELECTRIC LAYERS AND METAL STRIPE

Variations in the mode index and distribution of its fields were considered for both high and low index dielectric layers in Sec. IV for three different thicknesses of the dielectric layers. It was emphasized that despite the fact that the real part of the mode index, and therefore confinement in terms of distance from the cladding light line, increases or decreases in a monotonic fashion with increasing the dielectric layer thickness for high or low index dielectric layer, respectively, the spatial extent of the mode's fields in the vertical direction does not necessarily follow this pattern. This will be made clear in the investigation of the dependence of the mode's propagation range and spatial extent as a function of the thickness of the dielectric layers for both high and low index cases.

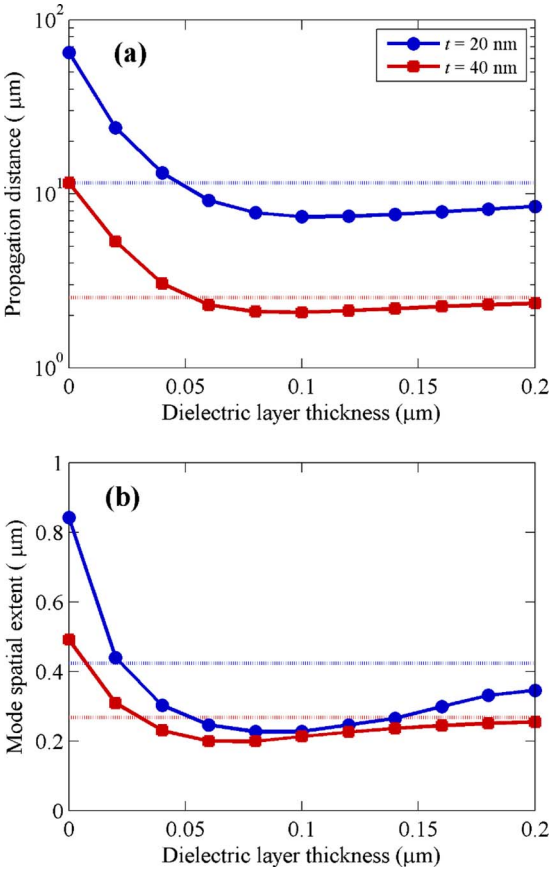


FIG. 7. (Color online) (a) Propagation range and (b) mode spatial extent in $y$ as a function of the dielectric layer thickness for high index dielectric layers. Dashed lines indicate the calculation results for the same metal stripe but embedded in a homogeneous background (no dielectric layers) of the high refractive index material ($n=2.0$).

### A. High index dielectric layers

The discussion on Sec. IV noted the increase in mode index with dielectric layer thickness for high index dielectric layers. First, this increases the rate at which the exponential tails of the mode's fields extend into the cladding decay, thereby reducing the mode size. In addition, due to the change in the functional form of the field distribution in the dielectric layers, effects of increases in the dielectric layer thickness are slightly more complex, as shown in Fig. 7. Calculations of the mode propagation range and spatial extent in the vertical dimension are shown for cladding and dielectric layer refractive indices of 1.50 and 2.00, respectively. The gold stripe is 1 $\mu$m wide and results for both 20 and 40 nm thick stripes are shown. The wavelength is 633 nm as in Sec. IV. Significantly, both the mode propagation range and spatial extent can be seen to reach a minimum confinement at the optimal point being improved over geometries with thicker dielectric layers, as well as the mode size of a stripe embedded in a purely homogeneous background of refractive index 2.00, shown as the dotted lines in the figure. We note that the solutions do not asymptote to these lines as the dielectric layer thickness approaches infinity, since for the geometry shown in Fig. 1 there will still be some of the $n_1=1.50$ material on the sides. The qualitative behavior is the same for increasing metal stripe thicknesses, although propagation range and spatial extent are reduced as a result of the reduced coupling of the SPPs propagating along long edges of the metal stripe for the thicker metal stripe, as is characteristic of the $ss_b^0$ mode.[7,8] The optimal thickness in terms of the mode confinement in the vertical dimension is reduced for the thicker metal stripe. The optimal thickness for the 20 nm thick gold stripe is roughly between 80 and 100 nm and is reduced to between 60 and 80 nm for the 40 nm thick gold stripe.

Since managing the tradeoff between propagation losses and mode confinement is a major concern in the design of plasmonic waveguide components, it is important to examine the effect quantitatively. For the 20 nm thick gold stripe, the mode spatial extents are 0.86, 0.23, and 0.42 $\mu$m for the $d=0$ (homogeneous low index background) point, $d=80$ nm point, and homogeneous high index background, respectively. The corresponding propagation distances are 65, 7.8, and 12 $\mu$m in the same order. For the 40 nm thick film, values are shifted toward higher loss and localization with the mode propagation distance and spatial extent combination being 12 and 0.49 $\mu$m, respectively, at the $d=0$ point. Values are reduced to 2.1 and 0.20 $\mu$m at $d=80$ nm and are 2.5 and 0.27 $\mu$m for the case of a homogeneous background made of high index material. Beyond the clear improvement in mode confinement in terms of its spatial extent, access to more favorable combinations of propagation range and mode size is a key feature of the guiding structure. If one already compares the mode sizes for the 20 nm thick film at the $d=80$ nm point and for the stripe without the dielectric layers, but embedding in the high index cladding, one finds a nearly twofold reduction of 0.23 $\mu$m as compared to 0.42 $\mu$m. At the same time, propagation range is only reduced from 12 to 7.8 $\mu$m. Although the thickness of the metal stripe might also be increased to improve the confinement without the use of the high index dielectric layers, the combination of mode spatial extent and propagation range achieved is significantly worse. This is evident when considering the propagation range and spatial extent in the vertical for the 20 nm thick gold stripe with 60 nm thick high index dielectric layers. The spatial extent is comparable to that of the 40 nm thick metal stripe embedded in a homogeneous background of the high index material, although the propagation range is much greater. Similar effects have been found if one considers combinations of propagation range and losses incurred after the mode has turned a 90° bend instead of propagation range and spatial extent.[31] The addition of the thin dielectric layers to the basic metal stripe geometry thus provides an important advantage in that more effective management of the tradeoff between propagation range and mode confinement is possible.

Although the monotonic increase in mode index and therefore distance from the cladding light line does imply improvements in mode confinement, it is the direct modification of the field distribution by the high index dielectric layers that accounts for the key feature illustrated in Fig. 7 and discussed in the preceding paragraph. The change in the field distribution is clear in Fig. 8, which shows the $H_x$ field profiles for the $d=0$ and $d=80$ nm points for the 20 nm thick metal stripes and also the gold stripe without dielectric layers

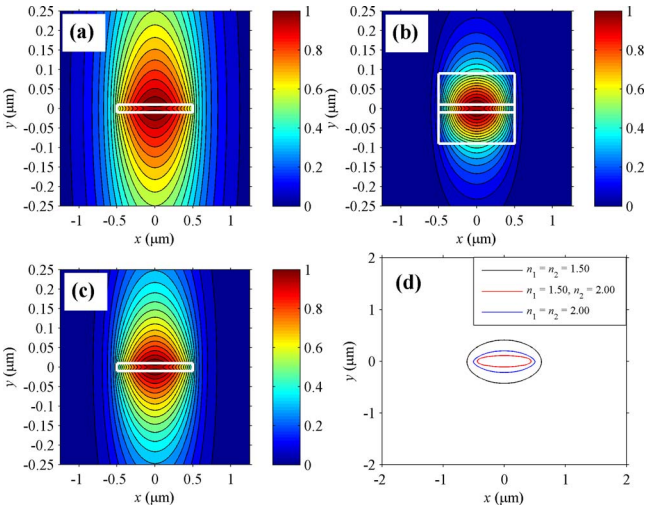


FIG. 8. (Color online) Profiles of the $H_x$ field component for the 20 nm thick gold stripe. Gold stripes in a homogeneous background without the inner dielectric layers are shown in (a) and (c) for cladding refractive indices of 1.50 and 2.00, respectively. The guide with 80 nm thick dielectric layers is shown in (b). The $1/e$ field contours are compared in (d).

in a homogeneous cladding with a refractive index of 2.00. The $1/e$ contours are also shown in Fig. 8(d). In Sec. III A, SPP dispersion curves were shown to lie to the lower momentum side of the dielectric layer light line at lower frequencies and where the metal stripe was relatively thin. With increasing frequency dispersion curves were seen to cross over the dielectric layer light line and it was noted that since the mode index of the $ss_b^0$ mode increases with the thickness of the metal stripe, the range of frequencies over which the wave vector of the SPP is greater than that of propagating radiation in the high index dielectric layer will be larger for thicker metal stripes. In Sec. IV the real part of the mode index was seen to increase with the thickness of the high index dielectric layers. The wave vector at $d=0$ for the 20 and 40 nm thick stripes examined here lies to the lower momentum side of the dielectric layers' light line. As the thickness of the high index dielectric layer is increased, the mode transitions from a hybrid mode, its field dependence in the $y$ direction being primarily cosine and sine functions in the dielectric layer, to a pure SPP, represented by exponential functions of the $y$ coordinate in the dielectric layer. For the 20 nm thick gold stripe, the real part of the mode index is below that of the dielectric layer refractive index until their thickness is brought to 200 nm, while for the 40 nm thick stripe, the mode index is already greater than 2.0 at $d=80$ nm. Although the mode is a hybrid at the optimal points for both metal stripe thicknesses, we note that confinement is improved over the homogeneous cladding case (dotted lines in Fig. 7) even as the mode becomes a pure SPP. The increase in mode index can be seen to reduce the mode size in the horizontal dimension as well. Since the form of the field distribution in the $x$ direction remains essentially unchanged by the dielectric layers, the spatial extent in the $x$ direction steadily decreases along with the increase in mode index varying from 1.2 at $d=0$ to 0.88 when $d=80$ nm to 0.87 $\mu$m at $d=200$ nm for the 20 nm thick metal stripe. Additionally, we note that for the geometry considered here, the horizontal

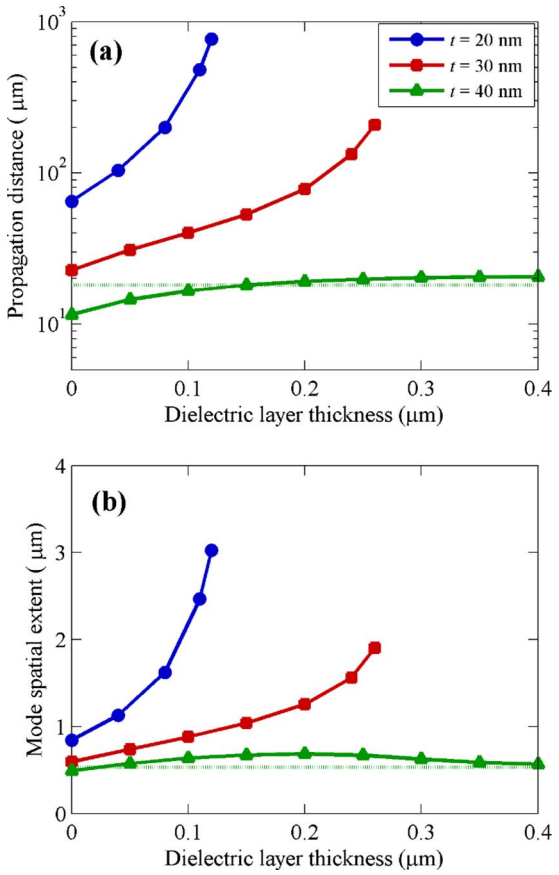


FIG. 9. (Color online) (a) Propagation range and (b) mode spatial extent in the vertical dimension for the low index dielectric layer case. The dashed line corresponds to the solution for the 40 nm thick gold stripe with $d=\infty$.

spatial extent is also improved over the homogeneous background case as a result of the greater contrast between the real part of the mode index and the cladding refractive index.

### B. Low index dielectric layers

The effects of increases in the dielectric layer thickness where their index of refraction is lower than that of the cladding are significantly different than for the high index case. The general effects have been discussed for one dimensional metal film guides in Refs. 25 and 26 and for a fixed thickness of the metal stripe for the two dimensional case in Ref. 28. The behavior for the finite width case is illustrated here for different stripe thicknesses in Fig. 9, which plots the mode propagation range and spatial extent in the $y$ direction. The stripe is 1 $\mu$m wide and the cladding and dielectric layer refractive indices are 1.50 and 1.45, respectively. The wavelength is again 633 nm. For the 20 and 30 nm thick metal stripes shown, increasing the layer thickness reduces mode confinement, and at the same time increasing propagation range. Eventually the mode is driven over the cladding light line and is cut off. As the dielectric layer thickness is increased toward the cutoff, propagation range improves significantly although as a result of the mode's fields becoming increasingly delocalized in and about the metal stripe. A significant fact here is that as can be seen in Fig. 9(a), through the use of low index dielectric layers it is even possible to extend the propagation range of a thicker, 30 nm for the case

here, stripe to and beyond that which is achievable with very thin films, which may be more challenging to fabricate. It is also clear from Fig. 9(b), however, that all things being equal, more favorable propagation range and spatial extent combinations result from modification of the stripe thickness as opposed to the use of dielectric layers. This highlights an interesting contrast between the low and high index dielectric layer cases, since in Sec. V A, it was shown that the use of high index dielectric layers achieves mode spatial extent and propagation range combinations that are preferable to those achieved with increasing stripe thickness. With increasing thickness of the metal stripe, the $ss_b^0$ mode becomes much more highly localized as the coupling between the top and bottom metal-dielectric interfaces is reduced. For the 40 nm thick metal stripe, in contrast to the behavior seen for the 20 and 30 nm thick stripes, propagation range can be seen to increase slightly, but the drastic gains associated with the cutoff are not apparent. For the tightly bound mode no increase in the thickness of the low dielectric layers will drive the dispersion curve over the cladding light line at the frequency and cladding-dielectric layer refractive index combination considered here. The mode remains bound for infinitely thick dielectric layers (dashed line in Fig. 9) and the spatial extent and propagation range can be seen to approach this value as the dielectric layers begin to extend well beyond the decay length of the fields of the mode and further increases in their thickness have little added effect. Increasing the contrast between the cladding and dielectric layers' refractive indices could allow for similar effects to be had for the 40 nm thick metal stripe as were shown for the thinner ones.

## VI. DEPENDENCE OF MODE PROPERTIES ON THE WIDTH OF THE METAL AND DIELECTRIC LAYERS

### A. High index dielectric layers

For high index dielectric layers, increases in their thickness can be viewed as raising the effective index in the region defined by their lateral width which, leveraging intuition from the behavior of dielectric waveguides,[46] will tend to concentrate the fields more tightly in the horizontal dimension. As can be seen from the field distribution in Fig. 8(b), the mode is very tightly concentrated to the center of the stripe in the horizontal dimension, the fields decaying to $1/e$ of the maximum value in the $x$ direction well inside the physical extent of the metal stripe. Since the horizontal extent of the mode implies the proximity with which guides deposited on a plane may be placed next to each other, the potential to use narrower guides is of interest. Figure 10 shows the variation in mode size and propagation range as the width of the gold stripe is varied from 1 to 0.08 $\mu$m. For stripe widths of 0.5 $\mu$m and larger, the mode's fields are concentrated along the $x$ direction almost entirely within the boundaries of the stripe edges. Hence, both propagation range and spatial extent in the $y$ direction deviate little as the stripe width is reduced. Spatial extent in the horizontal is dominated by dielectric waveguidelike effects resulting from the reduction in the physical stripe width. With further reductions in the stripe width, the $1/e$ decay points in the $x$ direction extend progressively further outside the metal stripe. The increased concentration of the mode's fields outside of the metal gives rise to the greater rate of increase in propagation range, and the reduced rate of exponential decay in the cladding causes increased spatial extents in the vertical dimension. A minimum is reached at $w=0.15$ $\mu$m for the spatial extent in the $x$ direction. Subsequent reductions in stripe width serve to lower the mode index to the point that the exponential decay of the field distribution in the cladding becomes the dominant factor in determining the spatial extent of the mode in both the $x$ and $y$ directions. Further reductions in the width of the metal stripe are expected to result in drastic increases in the mode's lateral size in analogy with the curves calculated and verified experimentally in Ref. 17 for a metal stripe embedded in a homogeneous background.

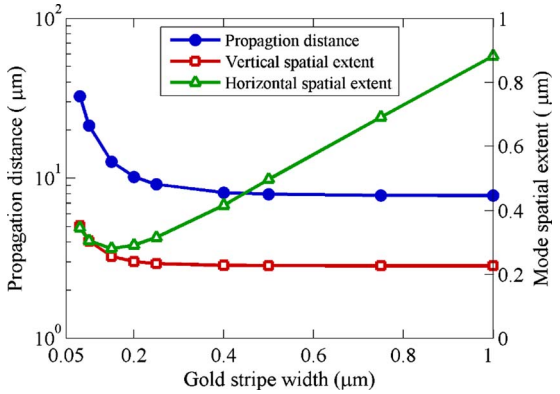


FIG. 10. (Color online) Propagation range and mode size for a 20 nm thick metal stripe guide of varying width with 80 nm thick high index ($n_2=2.0$) dielectric layers. The wavelength is 633 nm.

### B. Low index dielectric layers

While the high index dielectric layers increased the effective index in the region between the vertical edges of the metal strip, the low index dielectric layers lower it. The effects are shown in Fig. 11, which, analogous to Fig. 10, plots the mode propagation range and spatial extent in both $x$ and

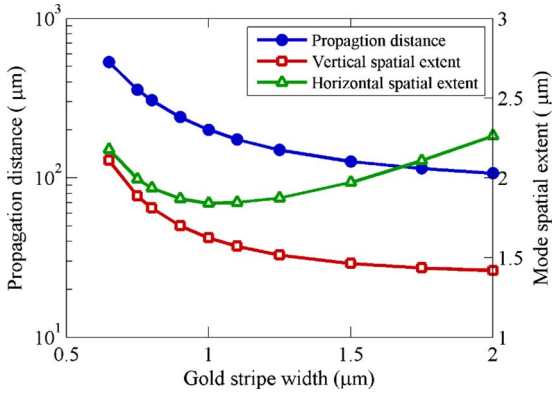


FIG. 11. (Color online) Propagation range (left axis) and mode spatial extent (right axis) in the vertical dimension and horizontal dimension as a function of the width of the gold stripe and dielectric layers. The thickness of the low index dielectric layers is set at $d=80$ nm. The wavelength is 633 nm.

$y$ as functions of the gold stripe's width for 80 nm thick dielectric layers having a refractive index of $n_2=1.45$. The cladding refractive index is 1.50 and the metal stripe is 20 nm thick. The wavelength is kept at 633 nm as well. In contrast to the high index dielectric layer case, where for gold stripe widths of greater than about 0.5 $\mu$m the majority of the mode's fields were concentrated well within the vertical edges of the metal stripe, for the low index dielectric layers, the mode is wider than the metal stripe even when it is 2 $\mu$m wide. As a result, increases in the propagation range and spatial extent in the vertical dimension of the mode with reductions in the metal stripe width are significantly larger than those seen for the high index dielectric layers. Although the spatial extent in the $x$ direction initially decreases with the width of the metal stripe as well, the minimum occurs for much wider metal stripes, about 1 $\mu$m in comparison with 150 nm, than for the guide with the high index dielectric layers. Furthermore, the comparison of Fig. 11 with Fig. 10 shows all the characteristics in the vicinity of the minimum horizontal mode size, propagation range, and spatial extent of the mode to be shifted to significantly higher values for the low index dielectric layers. Finally, because the mode wave vector decreases with the width of the metal stripe, the fact that the low index dielectric layers shift it toward the light line implies the presence of a nonzero metal stripe width below which the mode is cut off. Evidence of this can be seen in the drastic increases in the propagation range and mode size as the gold stripe width approaches 0.5 $\mu$m. For thicker dielectric layers, thinner gold stripes, greater contrasts between the cladding and the dielectric layers, or at longer wavelengths, this cutoff is expected to occur at increasingly larger widths.

## VII. SUMMARY

We have given a general systematic numerical analysis of the properties of the symmetric SPP mode supported by a thin metal stripe, above and below which thin dielectric layers are placed. We have shown that high or low index thin dielectric layers cause shifts in the $ss_b^0$ mode dispersion curves and perturb its field distribution, effects that translate to variations in the important mode characteristics of propagation range, and spatial confinement. Low index of refraction dielectric layers was shown to significantly extend the propagation range of the mode with the tradeoff of reduced confinement. High index layers can be used to enhance the mode confinement with mode sizes reduced well below those achievable with a homogeneous cladding of the high index material. Additionally, the high index dielectric layer configuration was found to allow for a more favorable exchange between loss and localization. The layered metal-dielectric structure investigated here presents a more versatile plasmonic waveguide geometry than that of a simple metal stripe embedded in a homogeneous dielectric background. The various tradeoffs and effects associated with the geometry discussed here can thus be leveraged to achieve long range plasmonic waveguides that are more carefully optimized with regard to given specific applications. Finally, we note that the calculations in Sec. IV illustrate that properly selected geometry and material parameters allow for a small change of the refractive index of the dielectric layers to result in relatively large effect in terms of the mode confinement and the propagation range. These effects may find useful applications for active plasmonic optical devices.

This work was partially supported by the National Science Foundation (NSF) and National Aeronautics and Space Administration (NASA) through the EPSCOR programs.

[1] H. Raether, *Surface Plasmons on Smooth and Rough Surfaces and on Gratings* (Springer-Verlag, Berlin, 1988).
[2] E. N. Economou, Phys. Rev. **182**, 539 (1969).
[3] D. Sarid, Phys. Rev. Lett. **47**, 1927 (1981).
[4] J. J. Burke, G. I. Stegeman, and T. Tamir, Phys. Rev. B **33**, 5186 (1986).
[5] B. Prade, J. Y. Vinet, and A. Mysyrowicz, Phys. Rev. B **44**, 13556 (1991).
[6] F. Yang, J. R. Sambles, and G. W. Bradberry, Phys. Rev. B **44**, 5855 (1991).
[7] P. Berini, Opt. Lett. **24**, 1011 (1999).
[8] P. Berini, Phys. Rev. B **61**, 10484 (2000).
[9] P. Berini, Phys. Rev. B **63**, 125417 (2001).
[10] B. Lamprecht, J. R. Krenn, G. Schider, H. Ditlbacher, M. Salerno, N. Felidj, A. Leitner, F. R. Aussenegg, and J. C. Weeber, Appl. Phys. Lett. **79**, 51 (2001).
[11] S. J. Al-Bader, IEEE J. Quantum Electron. **40**, 325 (2004).
[12] A. Degiron and D. R. Smith, Opt. Express **14**, 1611 (2006).
[13] The convention used here is to label the mode even or odd based on the symmetry of the spatial distribution of its dominant transverse electric or magnetic field components as in Refs. 7 and 8 above.
[14] R. Charbonneau, P. Berini, E. Berolo, and E. Lisicka-Skrek, Proc. SPIE **4087**, 534 (2000).
[15] P. Berini, R. Charbonneau, N. Lahoud, and G. Matiussi, J. Appl. Phys. **98**, 043109 (2005).
[16] P. Berini, R. Charbonneau, N. Lahoud, and G. Matiussi, Opt. Express **13**, 6298 (2005).
[17] A. Boltasseva, T. Nikolajsen, K. Leosson, K. Kjaer, M. S. Larsen, and S. I. Bozhevolnyi, J. Lightwave Technol. **23**, 413 (2005).
[18] A. Boltasseva, S. I. Bozhevolnyi, T. Sondergaard, T. Nikolajsen, and K. Leosson, Opt. Express **13**, 4237 (2005).
[19] I. Breukelaar, R. Charbonneau, and P. Berini, J. Appl. Phys. **100**, 043104 (2006).
[20] T. Nikolajsen, K. Leosson, and S. I. Bozevolnyi, Appl. Phys. Lett. **85**, 5833 (2004).
[21] T. Nikolajsen, K. Leosson, and S. I. Bozhevolnyi, Opt. Commun. **244**, 455 (2005).
[22] A. Karalis, E. Lidorikis, M. Ibanescu, J. D. Jouannopoulos, and M. Soljacic, Phys. Rev. Lett. **95**, 063901 (2005).
[23] M. I. Stockman, Nano Lett. **6**, 2604 (2006).
[24] G. Webb-Wood and P. G. Kik, Appl. Phys. Lett. **92**, 133101 (2008).
[25] J. Guo and R. Adato, Opt. Express **14**, 12409 (2006).
[26] R. Adato and J. Guo, Opt. Express **15**, 5008 (2007).
[27] R. Adato and J. Guo, Proc. SPIE **6641**, 66410G (2007).
[28] J. Guo and R. Adato, Opt. Express **16**, 1232 (2008).
[29] G. I. Stegeman and J. J. Burke, J. Appl. Phys. **54**, 4841 (1983).
[30] P. Berini, J. Appl. Phys. **102**, 033112 (2007).
[31] A. Degiron, C. Dellagiacoma, J. G. McIlhargey, G. Shvets, O. J. F. Martin, and D. R. Smith, Opt. Lett. **32**, 2354 (2007).
[32] Z. Sun, Appl. Phys. Lett. **91**, 111112 (2007).
[33] A. Degiron, S.-Y. Cho, C. Harisson, N. M. Jokerst, C. Dellagiacoma, O. J. F. Martin, and D. R. Smith, Phys. Rev. A **77**, 021804(R) (2008).
[34] P. Berini, Opt. Express **14**, 13030 (2006).
[35] J. Takahara, S. Yamagishi, H. Taki, A. Morimoto, and T. Kobayashi, Opt. Lett. **22**, 475 (1997).
[36] R. Zia, M. D. Selker, P. B. Catrysse, and M. L. Brongersma, J. Opt. Soc. Am. A Opt. Image Sci. Vis **21**, 2442 (2004).
[37] P. B. Johnson and R. W. Christy, Phys. Rev. B **6**, 4370 (1972).
[38] J. A. Dionne, L. A. Sweatlock, H. A. Atwater, and A. Polman, Phys. Rev. B **73**, 035407 (2006).
[39] *FIMMWAVE Version 4.5 Reference Manual* (Photon Design Ltd., Oxford, United Kingdom, 2006).
[40] A. S. Sudbo, Pure Appl. Opt. **2**, 211 (1993).
[41] A. S. Sudbo, Pure Appl. Opt. **3**, 381 (1994).

[42]P. Bienstman, S. Selleri, L. Rosa, H. P. Uranus, W. C. L. Hopman, R. Costa, A. Melloni, L. C. Andreani, J. P. Hugonin, P. Lalanne, D. Pinto, S. S. A. Obayya, M. Dems, and K. Panajotov, Opt. Quantum Electron. **38**, 731 (2006).
[43]L. Wendler and R. Haupt, J. Appl. Phys. **59**, 3289 (1986).
[44]P. Berini, J. Appl. Phys. **102**, 053105 (2007).
[45]F. Y. Kou and T. Tamir, Opt. Lett. **12**, 367 (1987).
[46]R. Zia, A. Chandran, and M. L. Brongersma, Opt. Lett. **30**, 1473 (2005).